Inorganic Chemistry

Article

pubs.acs.org/IC

Dicyclopalladated Complexes of Asymmetrically Substituted Azobenzenes: Synthesis, Kinetics and Mechanisms

Marina Juribašić,*[,†] Ana Budimir,[‡] Snježana Kazazić,[†] and Manda Ćurić*[,†]

[†]Division of Physical Chemistry, Ruđer Bošković Institute, Bijenička 54, HR-10000 Zagreb, Croatia

[‡]Faculty of Pharmacy and Biochemistry, University of Zagreb, Ante Kovačića 1, HR-10000 Zagreb, Croatia

Supporting Information

ABSTRACT: Two series of new dicyclopalladated complexes {(DMF)PdCl(μ-$R^1C_6H_3N{=}NC_6H_3R^2$)PdCl(DMF)} of 4,4′-functionalized azobenzenes with substituents of varying electron-donating or electron-withdrawing strength (R^1 = H, NMe_2; R^2 = H, Cl, Br, I, OMe, PhNH, CO_2H, SO_3Na, or NO_2) have been synthesized and fully characterized. ^{1}H NMR spectroscopy along with the ESI mass spectrometry unambiguously identified the new complexes in the solution, and their solid-state structures were determined by X-ray crystallography. The presence of easily exchangeable solvent ligands was confirmed by ^{1}H NMR spectroscopy, X-ray experiments, and ESI mass spectrometry. The complexes were additionally characterized by UV−vis and fluorescence spectroscopies. The effect of different 4,4′-substituents on the formation rate of mono- and dicyclopalladated azobenzenes was studied by UV−vis spectroscopy. The experimental results are complemented by the quantum-chemical (DFT) calculations in order to rationalize the kinetic results as well as substituent effects on the reaction rates. It was found that the mono- and dicyclopalladation reactions of azobenzenes proceed in two consecutive processes, adduct formation and palladation steps. The rate-determining step in both palladations is the breaking of the *ortho* C−H bond, which has been confirmed as an electrophilic substitution process by Hammett correlations and DFT calculations.

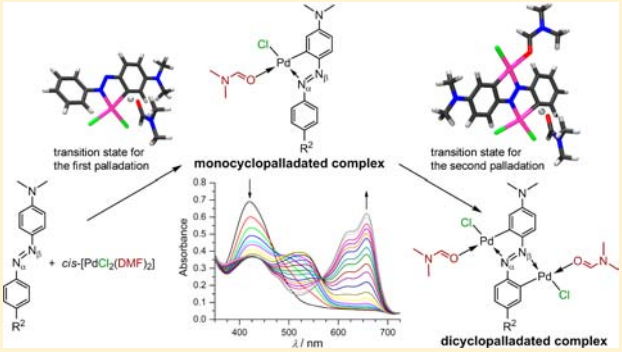

INTRODUCTION

Since the first report by Cope and Siekman,[1] cyclopalladated complexes of azobenzenes have been widely studied primarily because of their application in organic synthesis, in the design of liquid crystalline materials, new catalysts, and bioactive compounds.[2] Recently, we have focused our research efforts on the dicyclopalladated azobenzenes that absorb strongly in the visible region.[3] Some of them also emit even at room temperature in the solution as well as in the solid state.[3a] Such complexes contain two exchangeable solvent ligands[3] and thus may be used as precursors for a wide variety of new simple species or supramolecular systems relevant for sensors and optical devices.[4] Consequently, the photophysical properties of dipalladated azobenzenes can be easily modulated by appropriate selection of ancillary ligands as well as by varying the 4,4′-substituents on the azobenzene ligand.[4,5]

Although a number of synthetic studies of monocyclopalladated azobenzenes have been reported, experimental support for the cyclopalladation mechanism of azobenzenes is still lacking.[1,2e,i,6] The generally accepted cyclopalladation mechanism is the electrophilic substitution in which the hydrogen dissociation is often nucleophilically assisted by the coordinated or free bases, which accept the leaving proton.[7,8] In addition, the experimental data related to monocyclopalladation suggest that the phenyl ring with an electron-donating substituent is more favorable for *ortho*-cyclopalladation.[7d] Furthermore, adducts in which the Pd atom is bound to azobenzenes through coordinative bonds to the azo-nitrogen are generally assumed to be the first intermediates in the cyclopalladation process.[9] This assumption has been additionally supported by the studies of kinetics and cyclopalladation mechanisms of other N-donor ligands as well as by the quantum-chemical study of the cyclopalladation mechanism of azobenzene with $PdCl_2$ in *N*,*N*-dimethylformamide (DMF).[7] To the best of our knowledge, the kinetics of dicyclopalladation reaction has not been reported.

Herein we describe the synthesis and characterization of two novel series of dicyclopalladated complexes with azobenzenes, Scheme 1. Special attention was paid to the 4,4′-substituents on the azobenzene ligand, which play an important role in the structural and photophysical properties of dipalladated azobenzenes as well as in the kinetics of their cyclopalladation. In this context, a comparative kinetic study of the reaction of $PdCl_2(DMF)_2$ with azobenzene and its asymmetrically substituted derivatives in DMF was performed for the first time. The results of kinetic experiments complemented by the quantum-chemical calculations enabled better insight into the

Received: August 5, 2013
Published: October 11, 2013

   dx.doi.org/10.1021/ic402017v | *Inorg. Chem.* 2013, 52, 12749−12757

Scheme 1

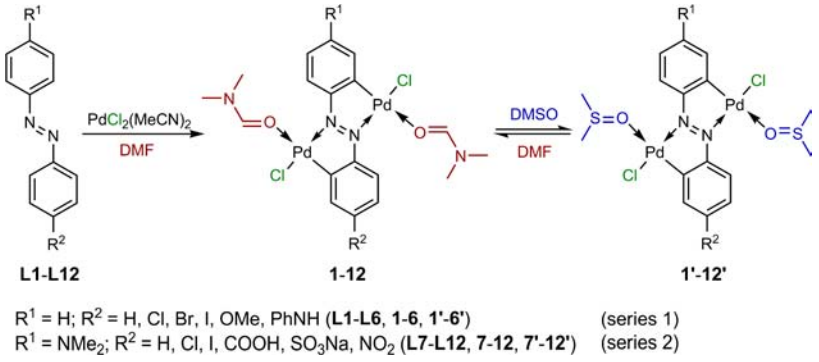

mechanism of dicyclopalladation reaction of azobenzenes as well as the reactivity of all species involved in this reaction.

EXPERIMENTAL SECTION

General. All chemicals were used as supplied and the reactions were carried out under aerobic conditions. Dicyclopalladated azobenzenes, {(DMF)PdCl(μ-$R^1C_6H_3N{=}NC_6H_3R^2$)PdCl(DMF)} (**2**−**11**), were prepared and characterized according to the previously reported procedure.[3] The ^{1}H NMR spectra were recorded at 25 °C in dimethyl sulfoxide-d_6 (DMSO-d_6) with a Bruker AV-600 spectrometer operating at 600.13 MHz. The atom numbering of azobenzenes used in the assignment of NMR resonances is given in Scheme S1, Supporting Information. Electronic absorption spectra were recorded on a Hewlett-Packard 8425 spectrophotometer in DMSO at 25 °C with a thermostatted cell compartment. Fluorescence spectra were recorded on a Varian Eclipse spectrophotometer in DMSO at 25 °C. Fluorescence in the solid-state was detected at 25 °C by confocal microscope LEICA/TCS/SP2 using nujol mull of samples with appropriate excitation wavelengths. Elemental analyses were carried out with a Perkin-Elmer series II 2400 CHNS/O analyzer.

Crystal Structure Determination. Single crystals of **2** and **5** were grown from DMF solutions, while those of **3**′, **6**′, and **8**′ were prepared by dissolving **3**, **6**, and **8** in DMSO. The X-ray measurements were performed on an Oxford Diffraction Xcalibur Nova R (microfocus Cu tube) at room temperature. The program package CrysAlisPRO[10a] was used for data reduction. The structures were solved using SHELXS97[10b] and refined with SHELXL97.[10c] Molecular geometry calculations were performed by PLATON,[10d] and molecular graphics were prepared using ORTEP-3[10e] and CCDC-Mercury.[10f] Crystallographic and refinement data for the structures reported in this paper are shown in Table S1, Supporting Information. CCDC 927924−927928 contain the supplementary crystallographic data for this paper. They can be obtained free of charge via www.ccdc.cam.ac.uk/conts/retrieving.html (or from the Cambridge Crystallographic Data Centre, 12, Union Road, Cambridge CB2 1EZ, UK, fax +44 1223 336033, or deposit@ccdc.cam.ac.uk).

ESI Mass Spectrometry. ESI mass spectra were recorded on an amaZon ETD ion trap mass spectrometer (Bruker Daltonik, Bremen, Germany). The compounds were dissolved in DMSO to obtain a concentration of approximately 10^{-4} mol/dm^3. The stock solution was diluted with MeCN to approximately 10^{-5} mol/dm^3 and injected into the ESI source. Helium was used as a collision gas.

Synthesis of Complexes. *{(DMF)PdCl(μ-$C_6H_4N{=}NC_6H_3Cl$)PdCl(DMF)}* (**2**). A mixture of 4-chloroazobenzene (50 mg, 0.23 mmol) and $PdCl_2(MeCN)_2$ (245 mg, 0.95 mmol) in DMF (4 mL) was stirred at room temperature for seven days. The dark red precipitate was filtered off and dried under vacuum. Yield: 78.0 mg, 52%. Calcd for $C_{18}H_{21}Cl_3N_4O_2Pd_2$: C 33.54, H 3.28, N 8.69. Found: C 33.14, H 3.43, N 8.21. The complex **2**′ was formed by dissolving complex **2** in DMSO. ^{1}H NMR (DMSO-d_6, δ/ppm, J/Hz): 7.87 d (H-3, ^3J(HH) = 7.9), 7.23 m (H-4,5), 8.75 br, s (H-6), 7.82 s (H-9), 7.36 d (H-11, ^3J(HH) = 7.8), 8.80 d (H-12, ^3J(HH) = 8.8). UV−vis (DMSO, λ_{max}/nm (ε/10^4 dm^3 mol^{-1} cm^{-1})): 315 (0.51), 407 (1.60), 440 sh (0.89), 553 (0.53), 585 (0.57). (+)ESI-MS (m/z): 618.5 [M − Cl]$^+$, 540.6 [M − Cl − DMSO]$^+$.

The complexes **3**−**11** were obtained by analogous reactions with the same ratio of azobenzenes and $PdCl_2(MeCN)_2$. The complexes **3**′−**11**′ were formed by dissolving **3**−**11** in DMSO, where DMSO displaces DMF as ancillary ligand. For ESI-MS, M = [Pd_2Cl_2(L-2H)$(DMSO)_2$].

{(DMF)PdCl(μ-$C_6H_4N{=}NC_6H_3Br$)PdCl(DMF)} (**3**). Yield: 85.0 mg, 64%. Calcd for $C_{18}H_{21}BrCl_2N_4O_2Pd_2$: C 31.38, H 3.07, N 8.13. Found: C 31.87, H 2.97, N 8.30. ^{1}H NMR (DMSO-d_6, δ/ppm, J/Hz): 7.88 d (H-3, ^3J(HH) = 9.9), 7.25 m (H-4,5), 8.77 br, s (H-6), 8.00 s (H-9), 7.51 d (H-11, ^3J(HH) = 8.8), 8.71 d (H-12, ^3J(HH) = 8.8). UV−vis (DMSO, λ_{max}/nm (ε/10^4 dm^3 mol^{-1} cm^{-1})): 314 (0.50), 410 (1.73), 439 sh (0.87), 555 (0.38), 588 (0.46). (+)ESI-MS (m/z): 664.6 [M − Cl]$^+$, 586.7 [M − Cl − DMSO]$^+$.

{(DMF)PdCl(μ-$C_6H_4N{=}NC_6H_3I$)PdCl(DMF)} (**4**). Yield: 91.1 mg, 76%. Calcd for $C_{18}H_{21}Cl_2IN_4O_2Pd_2$: C 29.37, H 2.88, N 7.61. Found: C 28.93, H 2.46, N 7.94. ^{1}H NMR (DMSO-d_6, δ/ppm, J/Hz): 7.87 d (H-3, ^3J(HH) = 9.2), 7.24 m (H-4,5), 8.77 br, s (H-6), 8.24 s (H-9), 7.70 d (H-11, ^3J(HH) = 8.6), 8.52 d (H-12, ^3J(HH) = 8.5). UV−vis (DMSO, λ_{max}/nm (ε/10^4 dm^3 mol^{-1} cm^{-1})): 313 (0.41), 416 (1.9), 443 sh (1.15), 560 (0.51), 594 (0.61). (+)ESI-MS (m/z): 664.7 [M − Cl]$^+$, 586.7 [M − Cl − DMSO]$^+$.

{(DMF)PdCl(μ-$C_6H_4N{=}NC_6H_3OMe$)PdCl(DMF)} (**5**). Yield: 120.0 mg, 80%. Calcd for $C_{19}H_{24}Cl_2N_4O_3Pd_2$: C 35.65, H 3.78, N 8.75. Found: C 35.89, H 3.34, N 8.35. ^{1}H NMR (DMSO-d_6, δ/ppm, J/Hz): 7.80 d (H-3, ^3J(HH) = 7.9), 7.16 t (H-4, ^3J(HH) = 7.7), 7.22 t (H-5, ^3J(HH) = 7.7), 8.59 d (H-6, ^3J(HH) = 7.8), 7.39 s (H-9), 6.85 d (H-11, ^3J(HH) = 9.1), 8.75 d (H-12, ^3J(HH) = 9.2), 3.87 s (OMe). UV−vis (DMSO, λ_{max}/nm (ε/10^4 dm^3 mol^{-1} cm^{-1})): 300 sh (0.60), 407 (1.49), 432 sh (1.20), 561 (1.18), 590 (1.18). (+)ESI-MS (m/z): 614.7 [M − Cl]$^+$, 536.7 [M − Cl − DMSO]$^+$.

{(DMF)PdCl(μ-$C_6H_4N{=}NC_6H_3NHPh$)PdCl(DMF)} (**6**). Yield: 64.5 mg, 50%; Calcd for $C_{24}H_{27}Cl_2N_5O_2Pd_2$: C 41.11, H 3.88, N 9.99. Found: C 41.60, H 3.39, N 9.59. ^{1}H NMR (DMSO-d_6, δ/ppm, J/Hz): 7.71 d (H-3, ^3J(HH) = 7.5 Hz), 6.93 t (H-4, ^3J(HH) = 7.6 Hz), 7.09 t (H-5, ^3J(HH) = 7.5 Hz), 8.37 d (H-6, ^3J(HH) = 8.9 Hz), 7.49 s (H-9), 6.80 d (H-11, ^3J(HH) = 9.2 Hz), 8.56 d (H-12, ^3J(HH) = 8.9 Hz), 7.27 d (H-14,18, ^3J(HH) = 8.0 Hz), 7.41 t (H-15,17, ^3J(HH) = 7.8 Hz), 7.15 t (H-16, ^3J(HH) = 7.4 Hz), 9.76 s (NH). UV−vis (DMSO, λ_{max}/nm (ε/10^4 dm^3 mol^{-1} cm^{-1})): 384 (0.60), 426 sh (0.40), 470 sh (0.29), 637 sh (1.48), 661 (1.64). (+)ESI-MS (m/z): 675.7 [M − Cl]$^+$, 597.8 [M − Cl − DMSO]$^+$.

{(DMF)PdCl(μ-$C_6H_4N{=}NC_6H_3NMe_2$)PdCl(DMF)} (**7**). Yield: 110.0 mg, 76%. Calcd for $C_{20}H_{27}Cl_2N_5O_2Pd_2$: C 36.77, H 4.17, N 10.72. Found: C 36.45, H 4.46, N 10.28. ^{1}H NMR (DMSO-d_6, δ/ppm, J/Hz): 7.68 d (H-3, ^3J(HH) = 7.7), 6.88 t (H-4, ^3J(HH) = 7.6), 7.05 t (H-5, ^3J(HH) = 7.6), 8.29 d (H-6, ^3J(HH) = 8.2), 7.23 s (H-9), 6.63 d (H-11, ^3J(HH) = 9.6), 8.51 d (H-12, ^3J(HH) = 9.6), 3.19 s (NMe_2). UV−vis (DMSO, λ_{max}/nm (ε/10^4 dm^3 mol^{-1} cm^{-1})): 312 (0.91), 382 (0.81), 441 sh (0.52), 478 sh (0.38), 623 (2.20), 656 (2.7). (+)ESI-MS (m/z): 627.9 [M − Cl]$^+$, 549.8 [M − Cl − DMSO]$^+$.

dx.doi.org/10.1021/ic402017v | Inorg. Chem. 2013, 52, 12749−12757

{(DMF)PdCl(μ-Me$_2$NC$_6$H$_3$N═NC$_6$H$_3$Cl)PdCl(DMF)} (**8**). Yield: 111.0 mg, 84%. Calcd for $C_{20}H_{26}Cl_3N_5O_2Pd_2$: C 34.93, H 3.81, N 10.18. Found: C 34.53, H 3.38, N 9.97. ^{1}H NMR (DMSO-d_6, δ/ppm, J/Hz): 7.24 s (H-3), 6.65 d (H-5, ^3J(HH) = 9.5), 8.50 d (H-6, ^3J(HH) = 9.0), 7.63 s (H-9), 7.13 d (H-11, ^3J(HH) = 8.8), 8.28 d (H-12, ^3J(HH) = 8.1), 3.19 s (NMe$_2$). UV−vis (DMSO, λ_{max}/nm (ε/10^4 dm^3 mol^{-1} cm^{-1})): 313 (1.75), 386 (1.37), 420 sh (1.04), 459 sh (0.84), 633 (3.89), 668 (4.91). (+)ESI-MS (m/z): 662.3 [M − Cl]$^+$.

{(DMF)PdCl(μ-Me$_2$NC$_6$H$_3$N═NC$_6$H$_3$I)PdCl(DMF)} (**9**). Yield: 98.0 mg, 88%. Calcd for $C_{20}H_{26}Cl_2IN_5O_2Pd_2$: C 30.83, H 3.36, N 8.99. Found: C 31.22, H 3.04, N 9.36. ^{1}H NMR (DMSO-d_6, δ/ppm, J/Hz) 7.22 s (H-3), 6.65 d (H-5, ^3J(HH) = 9.8), 8.50 d (H-6, ^3J(HH) = 9.4), 7.99 s (H-9), 7.44 d (H-11, ^3J(HH) = 8.4), 8.04 d (H-12, ^3J(HH) = 8.3), 3.19 s (NMe$_2$). UV−vis (DMSO, λ_{max}/nm (ε/10^4 dm^3 mol^{-1} cm^{-1})): 315 (0.63), 387 (0.44), 422 sh (0.29), 462 sh (0.19), 639 (1.43), 675 (1.83). (+)ESI-MS (m/z): 753.7 [M − Cl]$^+$, 675.7 [M − Cl − DMSO]$^+$.

{(DMF)PdCl(μ-Me$_2$NC$_6$H$_3$N═NC$_6$H$_3$COOH)PdCl(DMF)} (**10**). Yield: 108.0 mg, 83%. Calcd for $C_{21}H_{27}Cl_2N_5O_4Pd_2$: C 36.18, H 3.90, N 10.04. Found: C 35.69, H 3.45, N 10.34. ^{1}H NMR (DMSO-d_6, δ/ppm, J/Hz) 7.26 s (H-3), 6.70 d (H-5, ^3J(HH) = 9.5), 8.54 d (H-6, ^3J(HH) = 9.3), 8.23 s (H-9), 7.62 d (H-11, ^3J(HH) = 8.3), 8.29 d (H-12, ^3J(HH) = 8.2), 12.62 s (COOH), 3.22 s (NMe$_2$). UV−vis (DMSO, λ_{max}/nm (ε/10^4 dm^3 mol^{-1} cm^{-1})): 317 (1.31), 391 (0.85), 428 sh (0.58), 471 sh (0.39), 645 sh (3.20), 678 (3.87). (+)ESI-MS (m/z): 671.6 [M − Cl]$^+$, 593.7 [M − Cl − DMSO]$^+$.

{(DMF)PdCl(μ-Me$_2$NC$_6$H$_3$N═NC$_6$H$_3$SO$_3$Na)PdCl(DMF)} (**11**). Yield: 57.5 mg, 50%. Calcd for $C_{20}H_{26}Cl_2N_5O_5NaPd_2S$: C 31.81, H 3.47, N 9.27. Found: C 31.31, H 3.89, N 9.67. ^{1}H NMR (DMSO-d_6, δ/ppm, J/Hz) 7.20 s (H-3), 6.60 d (H-5, ^3J(HH) = 9.5), 8.49 d (H-6, ^3J(HH) = 9.4), 7.90 s (H-9), 7.27 d (H-11, ^3J(HH) = 8.4), 8.18 d (H-12, ^3J(HH) = 8.3), 3.16 s (NMe$_2$). UV−vis (DMSO, λ_{max}/nm (ε/10^4 dm^3 mol^{-1} cm^{-1})): 312 (1.12), 385 (0.89), 422 sh (0.58), 468 sh (0.38), 631 (2.66), 668 (3.30).

Kinetic Measurements. Reactions of the $PdCl_2(MeCN)_2$ complex with azobenzene (**L1**) and its asymmetrically substituted derivatives **L2**−**L12** were studied using UV−vis spectroscopy. The reactions were followed in the 350−780 nm range on a Cary 50 UV−vis spectrophotometer equipped with a multicell transport, thermostatted (±0.1 °C) with a Varian refrigerated circulation bath. All kinetics experiments were performed under the pseudo-first-order conditions, for which the concentration of $PdCl_2(MeCN)_2$ was always in at least a 20-fold molar excess. The reactions were initiated by mixing equal volumes of a DMF solution of azobenzene with a DMF solution of $PdCl_2(MeCN)_2$ in a simple 1 cm UV−vis cuvette. No salt was added to control the ionic strength. The observed pseudo-first-order rate constants, k_{obs}, were derived from absorbance vs time traces at the wavelengths where a maximum increase or decrease in absorbance was observed. No dependence of the values on the selected wavelengths was detected. The data were analyzed using Origin 7.5 and SPECFIT software.

Computational Details. All calculations were carried out using the Gaussian09[11] implementation of DFT B3LYP method.[12a] Full geometry optimizations of the minima and the transition states, along with the vibrational frequency calculations reported in this paper, were performed at the B3LYP/6-31G(d,p)-IEF-PCM level of theory. The standard 6-31G(d,p) basis set was used for C, H, N, O, Cl, Br, S, and Na atoms, whereas Pd and I atoms were modeled by the Stuttgart−Dresden (SDD) pseudopotential and the accompanying SDD basis set.[12b] DMF was modeled using the polarizable continuum model (IEF-PCM).[12c] The free energies were given at 298.15 K and 1 atm. The nature of the transition structures was also confirmed by the intrinsic reaction coordinate (IRC) searches.[12d] The prereaction complexes, afforded by the IRC calculations and followed by the geometry optimizations, were used for the evaluation of the free energies of activation in the adduct formation processes.

RESULTS AND DISCUSSION

Synthesis and Characterization. The general synthetic route to two series of dicyclopalladated azobenzenes **1**−**6** and **7**−**12** is described in Scheme 1.[3] The compounds **1**−**12** were isolated as microcrystalline solids, which are soluble in DMSO, DMF, and pyridine, while **1′**−**12′** were formed by dissolving **1**−**12** in DMSO. Although we do not have single crystal X-ray structures of **4**, **7**, and **9**−**11**, all spectral data support formulations of these complexes as dicyclopalladated compounds. ^{1}H NMR signals of aromatic protons confirmed the double cyclopalladation of azobenzenes (see Experimental Section). In the spectra recorded in DMSO-d_6, signals corresponding to the free DMF were observed since DMSO-d_6 displaces DMF.

ESI-MS studies have confirmed the fast exchange of solvent ligands in dicyclopalladated azobenzenes and the stability of dicyclopalladated moiety in the solution and in the gas-phase. Two signals assigned to $[Pd_2(L\text{-}2H)Cl(DMSO)_2]^+$ and $[Pd_2(L\text{-}2H)Cl(DMSO)]^+$ species were observed in (+)ESI spectra of all complexes, confirming that DMF ligands were exchanged with DMSO. Detailed fragmentation pathways of the complexes studied by collisional experiments (ESI MS^n) will be described elsewhere.

X-ray Analysis. The single-crystal X-ray structural results of complexes have revealed that the bond angles and distances related to the Pd environments, orientation of solvent and chloride ligands toward the Pd−C bond in new complexes, and their crystal packing are similar to those in dicyclopalladated azobenzenes reported previously, see Table S2, Supporting Information, and Figure 1 and Figures S1−S11, Supporting Information.[3] Thus, the solvent ligands are oriented *trans* to the Pd−C bond and bound to palladium through oxygen atoms. The Pd−O bond lengths are longer than the sum of covalent radii for oxygen and palladium due to the strong *trans* influence of the Pd−C bond, Table S2, Supporting Information. Furthermore, the C−H···O intramolecular hydrogen bonds, C−H···Cl−Pd hydrogen bonds, or C−H···Pd, π···π, and C−H···π interactions dominate in the crystal packing of **2**, **3′**, **5**, **6′**,

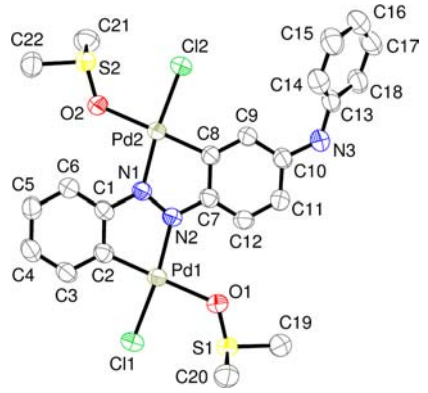

Figure 1. ORTEP view of **6′**. Displacement ellipsoids are shown at 50% probability level, and hydrogen atoms are omitted for clarity. Bond distances (Å): Pd1−Cl1, 2.3121(9); Pd1−N2, 2.057(2); Pd1−O1, 2.184(3); Pd1−C2, 1.957(3); Pd2−Cl2, 2.2974(9); Pd2−N1, 2.051(2); Pd2−O2, 2.160(3); Pd2−C8, 1.959(3). Bond angles: Cl1−Pd1−O1, 87.75(7)°; N2−Pd1−C2, 79.46(10)°; Cl2−Pd2−O2, 87.01(7)°; N1−Pd2−C8, 79.61(10)°. Dihedral angle: C10−N3−C13−C14, 42.7(5)°.

dx.doi.org/10.1021/ic402017v | *Inorg. Chem.* 2013, 52, 12749−12757

and **8′**, Tables S3−S4 and Figures S5−S11, Supporting Information.[3b,13]

Absorption and Emission Spectra. The UV−vis spectra recorded in DMSO are characterized by low energy bands that have higher intensity and are more red-shifted if the complex simultaneously contains electron-donating and electron-withdrawing groups. In view of the similar absorption bands observed in the spectra of other dicyclopalladated azobenzenes and their assignment made on the basis of TD-DFT calculations,[3b] the most intense absorption bands at 407−416 and 661−678 nm are assigned as intraligand (IL) $\pi^* \leftarrow \pi$ and metal to ligand charge transfer (MLCT) transitions. The energy trend of these absorption bands, **10′** < **9′** < (**8′**, **11′**) < **6′** < **4′** < **3′** < **2′** < **5′**, follows the degree of electron richness of the 4,4′-substituents on the azobenzene (NMe_2, COOH) > (NMe_2, I) > (NMe_2, SO_3Na), (NMe_2, Cl) > (H, PhNH) > (H, NMe_2,) > (H, I) > (H, Br) > (H, Cl) > (H, OMe). Upon photoexcitation, the complexes containing the amino group (PhNH or NMe_2), **6′**−**11′**, display emission bands in the low energy region at 703−722 nm in DMSO solution at room temperature, Table 1. The substituted azobenzenes *per se* do not luminesce either in the solution or in the solid state at room temperature; however, their dicyclopalladated complexes with dimethyl or phenylamino groups in the *para* position of azobenzene (**6**−**10**) show significant fluorescence in the solid state as detected by confocal microscopy, Table 1 and Figure S12, Supporting Information.

Table 1. Fluorescence Data[a]

compound	λ_{max}, excitation (nm)	λ_{max}, emission (nm)	
6′	680	722	DMSO
6	594, 633	660−720	solid
7′	670	688	DMSO
7	594, 633	750−833	solid
8′	680	703	DMSO
8	633	670−790	solid
9′	670	709	DMSO
9	633	670−730	solid
10′	690	712	DMSO
10	633	730−830	solid
11′	680	715	DMSO

[a]Complexes **6′**−**11′** are formed by dissolving complexes **6**−**11** in DMSO.

Mechanistic Study. Mono- and dicyclopalladation reactions of two series of ligands, **L1**−**L6** (series 1) and **L7**−**L12** (series 2), Scheme 1, have been studied experimentally and computationally for the first time.

Kinetics. The kinetics of reactions of the $PdCl_2(DMF)_2$ complex with azobenzene (**L1**) and its asymmetrically substituted derivatives **L2**−**L12** were studied spectrophotometrically in DMF in order to examine the influence of different 4,4′-substituents on the formation rate of dicyclopalladated products, Scheme 2. The $PdCl_2(DMF)_2$ complex was formed by dissolving the $PdCl_2(MeCN)_2$ in DMF.[6a] According to the calculations, *cis*-$PdCl_2(DMF)_2$ is thermodynamically favorable. The formation of two isomeric species (alpha and beta) was observed in ^{1}H NMR spectra of reactions with asymmetrically substituted azobenzenes due to similar affinities of two azo-nitrogens (N_α and N_β) toward Pd(II).[6a] However, the difference between the alpha and beta isomers is not visible in UV−vis spectra.

Kinetics measurements were carried out under the pseudo-first-order conditions with the $PdCl_2(DMF)_2$ complex in a large (usually 20−120-fold) molar excess. The time-resolved UV−vis spectra recorded during the reaction of $PdCl_2(DMF)_2$ with **L7** is shown in Figure 2. The reaction is characterized by two consecutive color changes assigned to the formation of mono- and dicyclopalladated complexes.

The sum of the two-exponential function (eq 1) was fitted to the observed absorbance versus time trace at suitable wavelengths with the amplitudes having opposite signs as shown in Figure S13, Supporting Information. The symbols ΔA_1 and ΔA_2 are the total absorbance changes (amplitudes) for the first and second process, while A_t and A_∞ are the absorbance at time t and infinite time, respectively.

$$A_t = \Delta A_1\, e^{-k_{obs1}t} + \Delta A_2\, e^{-k_{obs2}t} + A_\infty \qquad (1)$$

The pseudo-first-order rate constants, k_{obs1} and k_{obs2}, calculated from such kinetic traces were plotted vs the concentration of the $PdCl_2(DMF)_2$. In the case of the phenylamino- and all dimethylamino-substituted azobenzenes (**L6**−**L12**), both steps have excellent linear fits with zero

Scheme 2

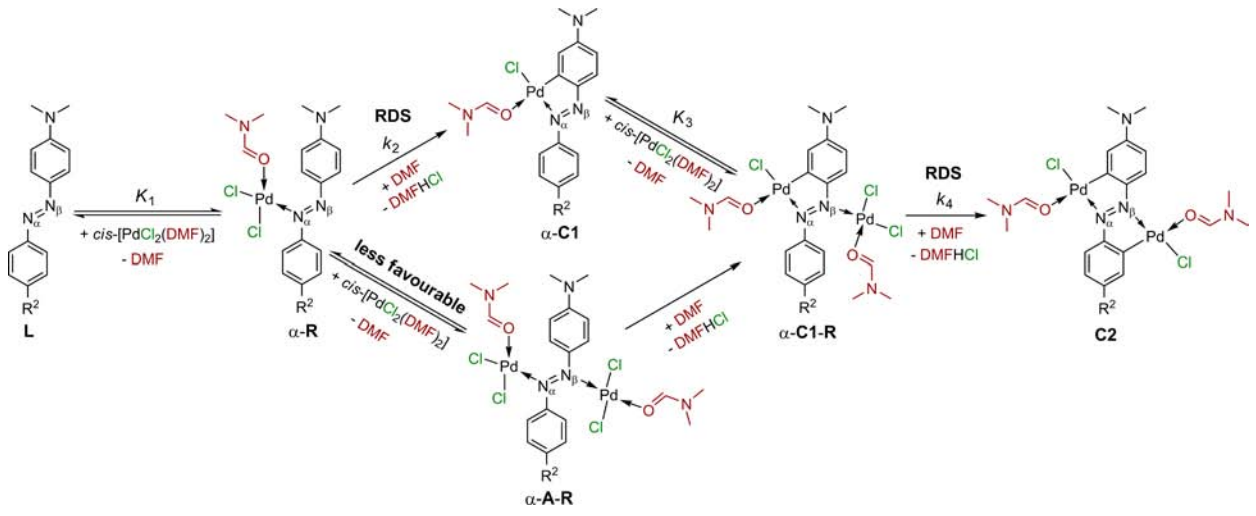

dx.doi.org/10.1021/ic402017v | Inorg. Chem. 2013, 52, 12749−12757

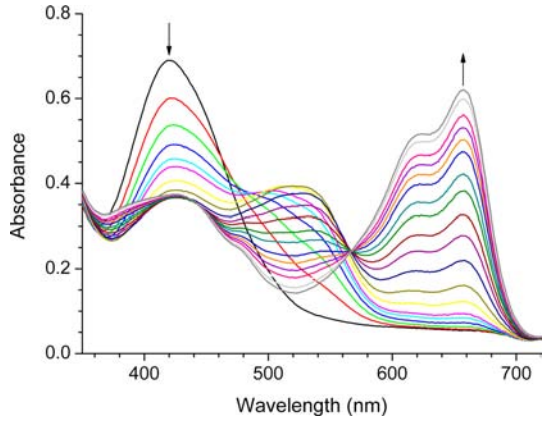

Figure 2. Spectral changes as a function of time during the reaction of $PdCl_2(DMF)_2$ with **L7** in DMF. $[PdCl_2(DMF)_2]$ = 1.2 mmol dm^{-3}, [**L7**] = 20 μmol dm^{-3}, optical path length = 1.00 cm, θ = 25.0 °C, reaction time intervals from 1 to 1200 min.

intercepts, indicating that the backward reactions can be neglected. The plots of the observed pseudo-first-order rate constants, k_{obs1} and k_{obs2}, vs the concentration of the $PdCl_2(DMF)_2$ for the two reaction steps of **L7** are shown in Figure 3.

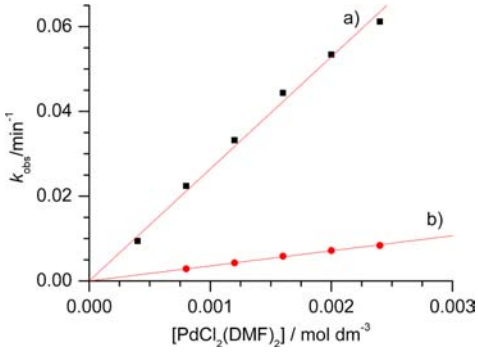

Figure 3. Dependence of the pseudo-first-order rate constants (a) k_{obs1} and (b) k_{obs2} on the $PdCl_2(DMF)_2$ concentration during the reaction of **L7** with $PdCl_2(DMF)_2$ in DMF. [**L7**] = 20 μmol dm^{-3}; θ = 25.0 °C.

The reaction of the $PdCl_2(DMF)_2$ with azobenzene (**L1**) and its monosubstituted derivatives **L2**–**L5** in the concentration range of the kinetic experiments led only to the monopalladated complexes. The second reaction was very slow even at 35 °C, and no reliable values of k_{obs2} were obtained; thus only the values of k_{obs1} were calculated and they also gave excellent linear fit vs. $PdCl_2(DMF)_2$ concentration with zero intercept. The observed rate constants for the two reactions can be expressed by the general eq 2.

$$k_{obs1} = k'[PdCl_2(DMF)_2] \quad (2a)$$

$$k_{obs2} = k''[PdCl_2(DMF)_2] \quad (2b)$$

Monocyclopalladation. The kinetic results obtained herein for the monocyclopalladated complexes (**C1**) are consistent with a reaction mechanism in which azobenzene (**L**) coordinates the Pd atom through the azo-nitrogen in the first fast pre-equilibrium step producing the mononuclear adduct $LPdCl_2(DMF)$ (α-**R**), from which the intramolecular C–H bond activation starts in the second rate-determining step, as shown in Scheme 2. ^{1}H NMR and computational studies of analogous reactions indicated that the adducts with two ligands were not present,[6,8] although such species were found as the first intermediates in the cyclopalladation of amines.[7]

According to Scheme 2, the dependence of the observed rate constant on $PdCl_2(DMF)_2$ concentration can be expressed as:

$$k_{obs1} = \frac{k_2K_1[PdCl_2(DMF)_2]}{1 + K_1[PdCl_2(DMF)_2]} \quad (3)$$

If the value of K_1 is rather low, which is most likely the case for the reactions investigated herein, then $K_1[PdCl_2(DMF)_2] \ll 1$, and the relation 3 becomes

$$k_{obs1} = k_2K_1[PdCl_2(DMF)_2] \quad (4)$$

This is in accordance with the observed linear k_{obs1} vs $PdCl_2(DMF)_2$ concentration dependence, Figure 3. By comparison of the eqs 2a and 4, it is obvious that $k' = k_2K_1$. The values of the product k_2K_1 determined by a linear fit of the experimental data are listed in Table 2. The formation of the

Table 2. Substituent Effects on the Rates of the First (k_{obs1}) and the Second (k_{obs2}) Cyclopalladation Reactions of Azobenzene Derivatives in DMF

	R^1	R^2	k_{obs1} (dm^3 mol^{-1} s^{-1})	k_{obs2} (dm^3 mol^{-1} s^{-1})
		Azobenzene Series (35.0 °C)		
L1	H	H	0.093(1)	–
L2	H	Cl	0.048(1)	–
L3	H	Br	0.0478(3)	–
L4	H	I	0.060(2)	–
L5	H	OMe	0.168(3)	–
L6	H	PhNH	0.557(6)–	–*a*,*b*
L7	H	NMe_2	0.77(1)	–*a*
		4-(*N*,*N*-Dimethylamino)azobenzene Series (25.0 °C)		
L7	NMe_2	H	0.440(2)	0.059(5)
L8	NMe_2	Cl	0.282(2)	0.033(1)
L9	NMe_2	I	0.388(3)	0.053(1)
L10	NMe_2	COOH	0.320(3)	0.055(3)
L11	NMe_2	SO_3Na	0.69(1)	0.072(1)
L12	NMe_2	NO_2	0.278(1)	0.034(1)

[a]Only the monocyclopalladation reaction is studied. [b]The rate constants for mono- and dicyclopalladation of **L6** at 25.0 °C are 0.310(2) and 0.0558(1) dm^3 mol^{-1} s^{-1}, respectively.

mononuclear adduct, $LPdCl_2(DMF)$, in the fast pre-equilibrium step is supported by the spectra recorded in a two-compartment cuvette, Figure S14, Supporting Information. Preliminary experiments showed that the adduct formation occurs on the stopped-flow time scale. Detailed study is in progress, and the results will be discussed elsewhere.

Dicyclopalladation. The formation of dicyclopalladated complex **C2** proceeds in an almost 10 times slower single step as suggested by the isosbestic point detectable at the later reaction times. As shown above, the pseudo-first-order rate constants, k_{obs2}, gave an excellent linear fit versus $PdCl_2(DMF)_2$ concentration with zero intercept. These kinetic findings could be explained by the comparison with the above proposed monocyclopalladation mechanism. Thus, the monopalladated complex (α-**C1**) coordinates the new $PdCl_2(DMF)_2$ through the free azo-nitrogen in the first fast pre-equilibrium step producing the monocyclopalladated adduct (α-**C1**-**R**) from which the intramolecular C–H bond activation starts in the second rate-determining step, as shown in Scheme 2.

dx.doi.org/10.1021/ic402017v | *Inorg. Chem.* 2013, 52, 12749–12757

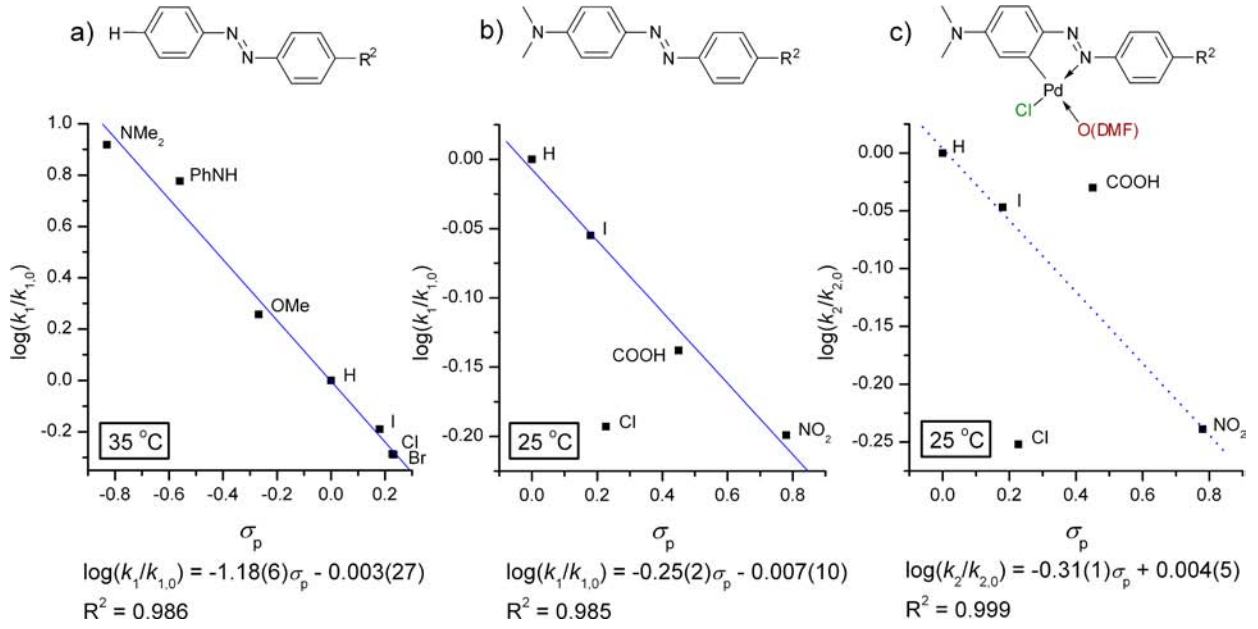

Figure 4. Substituent effects on the rates of the first cyclopalladation reaction for (a) monosubstituted azobenzenes (correlation data for $R^2 = NMe_2$, PhNH, OMe, H, I, Cl, and Br) and (b) dimethylaminoazobenzenes (correlation data for R^2 = H, I, CO_2H, and NO_2) and (c) the second cyclopalladation reaction for dimethylaminoazobenzenes (correlation data for R^2 = H, I, NO_2). Substituent R^2 is used for the graph point labeling. Values for **L11** ($R^2 = SO_3Na$) are not shown.

The linear dependence of k_{obs2} vs. $PdCl_2(DMF)_2$ concentration can be expressed by eq 5:

$$k_{obs2} = \frac{k_4K_3[PdCl_2(DMF)_2]}{1 + K_3[PdCl_2(DMF)_2]} \quad (5)$$

If we assume a low value for K_3 then $K_3[PdCl_2(DMF)_2] \ll 1$, and the relation 5 becomes

$$k_{obs2} = k_4K_3[PdCl_2(DMF)_2] \quad (6)$$

From eqs 2b and 6, it is evident that $k'' = k_4K_3$. The values of the product k_4K_3 determined by a linear fit of the experimental data for the 4-phenylaminoazobenzene (**L6**) and 4-dimethylaminoazobenzene ligands **L7**−**L12** are listed in Table 2.

Substituent Effects. Substituent effects on the mono- and dicyclopalladation of **L1**−**L12**, Scheme 1, have been studied for the first time with Hammett correlation plots.[14] Generally, electron-donating substituents increase the reaction rates, which is in agreement with the literature data.[7]

The rate constants at 35 °C for the monocyclopalladation of the azobenzene (**L1**) and its monosubstituted derivatives **L2**−**L7**, in which the varying substituents are bound to the palladated phenyl ring, increase in the order **L2**, **L3** < **L4** < **L1** < **L5** < **L6** < **L7**. Excellent Hammett correlation gives a considerably negative slope (ρ = −1.18), revealing the important role of the substituent in the transition state stabilization, Figure 4a.

The order of the rate constants for the monocyclopalladation of dimethylaminoazobenzenes **L7**−**L12** at 25 °C is **L12** < **L8** < **L10** < **L9** < **L7** < **L11**. Although the monocyclopalladation of these azobenzenes takes place on the phenyl ring with the same 4-substituent (NMe_2), the differences between the rate constants, as well as their order, indicate the influence of the 4′-substituent on the formation rate of monocyclopalladated azobenzenes. The Hammett plot gives a small but notable negative value ρ = −0.25, Figure 4b. This shows that even the substituents present in the phenyl ring that is not being palladated act through the whole azobenzene skeleton and influence the palladation reaction. The dicyclopalladation rate constants for the dimethylaminoazobenzenes show an analogous trend to their monocyclopalladation rate constants within statistical error, Table 2. The tentative slope −0.31 can be deduced for ligands **L7**, **L9**, and **L12** using *para*-constants, Figure 4c.

The negative slopes are consistent with the electrophilic substitution mechanism and agree well with the C−H bond breaking as the rate-determining step in both cyclopalladation reactions, Scheme 2. The linear correlation of the experimental rate constants for the first cyclopalladation reaction of both studied series is achieved only with *para*-Hammett constants, Figure 4. Poor *meta*- and *para*-Hammett correlations for the dicyclopalladation process indicate the possible influence of the formed cyclopalladated ring on the reaction rates. Furthermore, the adduct formation and the cyclopalladation step both contribute to the observed rate constant. Thus, the correlation can be perturbed since the substituents can affect both reaction sites, that is, the metal center (in *para*-position) and the C−H bond (in *meta*-position).

The mono- and dicyclopalladations of methyl orange (**L11**) give the highest rate constants of all studied ligands. The rates are much higher than the expected values from the Hammett plots; thus they are excluded from the correlations in Figure 4. The reason for this could be the partial dissociation of the *para*-substituent SO_3Na in DMF. This would lead to changes in the ionic strength, which may influence the rate of the cyclopalladation reactions. This issue will be addressed in our future mechanistic studies of azobenzene palladation.

Computational Studies. Experimental findings motivated us to carry out the computational study in order to provide a plausible explanation of the reaction mechanism and to rationalize the substitutent effects on the reaction rates. Ligand **L7** (R^1 = H, $R^2 = NMe_2$) was used for the detailed study including all species involved in both steps, that is, adduct

dx.doi.org/10.1021/ic402017v | Inorg. Chem. 2013, 52, 12749−12757

formation and cyclopalladation, while only the adduct formation and the C−H bond breaking were modeled for ligands **L8** and **L10**−**L12**. Monocyclopalladated complexes were modeled for all ligands. The computational modeling details are given in the Supporting Information.

Regioselectivity. Asymmetrically substituted azobenzenes in this study offer two regioisomers, since each phenyl ring can be palladated. Two reaction paths, alpha and beta, can be conceived and modeled, Schemes S2 and S3, Supporting Information. Because these paths cannot be easily distinguished experimentally, the differences between them have been assessed computationally. In general, the beta path has appeared as the energetically more demanding process. Thus, the reported data in this work correspond to the alpha path unless stated otherwise. The data suggest that the first palladation occurs on the phenyl ring with the electron-donating substituent, that is, NMe_2, which is in agreement with the literature[5b] and our experimental data.

The computational data are presented in three related sections: (i) monocyclopalladation, (ii) dicyclopalladation, and (iii) diadduct cyclopalladation.

Monocyclopalladation. Approach of *cis*-$PdCl_2(DMF)_2$ to the azobenzene species results in the trigonal-bipyramidal configuration around the palladium atom in the transition states *α*-**TS1** and *β*-**TS1**, Figures S15−S17, Supporting Information. The Pd−N distances vary in the range 2.67−2.71 Å, while the Pd−Cl bonds are not affected by the reaction. In this substitution reaction, one DMF ligand leaves the coordination sphere of the palladium, and the second DMF molecule stays attached in the *cis* position to the azobenzene species, with the Pd−O distances being 2.43−2.48 and 2.04−2.07 Å, respectively. Various conformations can be visualized for this type of transition state, and computations show that several are in a 10 kJ/mol range, for example, Figure S16, Supporting Information. Transition states in which the *trans*-$PdCl_2(DMF)_2$ approaches the azobenzene are 12−18 kJ/mol higher in energy than the *cis*-transition states, Table S5, Supporting Information.

The monoadduct formation is experimentally characterized as a fast process, and all spectroscopic data indicate that there is no backward reaction once adduct is formed. Since calculations give $\Delta G^{\ddagger}$ values of 63−66 kJ/mol and $\Delta_r G$ in the range from −50 to −55 kJ/mol for the adduct formation, the backward reaction can be ruled out, Figure 5 and Figures S21−S24, Supporting Information. In addition, the transition states *α*-**TS1** and *β*-**TS1** are close in energy, Table S5, Supporting Information, which allows the formation of both adducts. These data correspond nicely to the NMR studies, which showed two new sets of signals, assigned as two adduct species, emerging in the spectra immediately after mixing the DMF-d_7 solutions of ligand **L12** and $PdCl_2(MeCN)_2$.

The monocyclopalladation mechanism for the nonsubstituted azobenzene was studied by Babić et al.[8] The study ruled-out the coordinated chlorides and the solvent molecules from the bulk as the proton-accepting species and the dimeric adduct species as the reactants entering the cyclopalladation. The proton transfer was found to be the rate-determining step. We verified this mechanism as the most energetically favorable path for the mono- and dicyclopalladation of the dimethylamino-azobenzene ligands and used it throughout this study.

All modeled species included in the monocyclopalladion of the studied ligands, Scheme S2, Supporting Information, are conformationally similar to the published azobenzene species.[8] It should be mentioned here that although $LPdCl_2(DMF)$

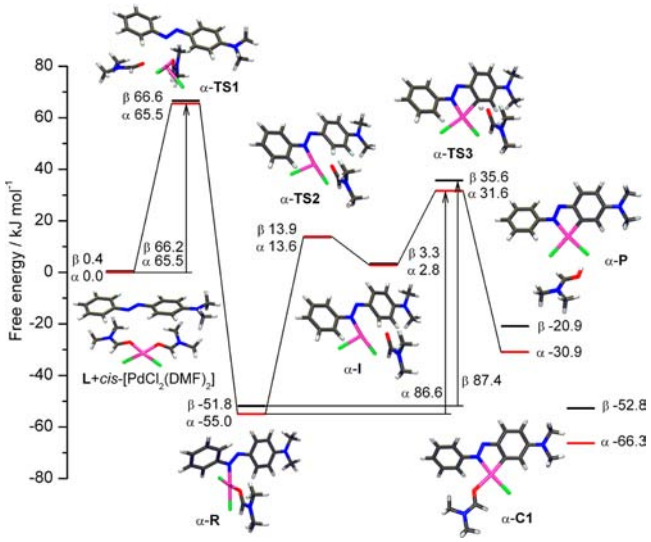

Figure 5. Energy profile for the monocyclopalladation reaction of **L7**. Alpha and beta paths are shown in red and black, respectively. Only alpha structures are drawn.

adduct complexes with the DMF molecule in *trans* position toward the azobenzene (*α*-**A**) are 5−6.5 kJ/mol more stable than *α*-**R** species, Table S6, Supporting Information, they cannot enter the energetically favorable DMF-assisted cyclopalladation without the isomerization to *α*-**R** species. The HCl is released from the product species *α*-**P** and *β*-**P**, most likely as DMF·HCl, and one DMF molecule from the bulk occupies the vacant coordinate place on the palladium forming *α*-**C1** and *β*-**C1**. This process is expected to occur fast; thus the corresponding transition states were not modeled. The calculations also show that *α*-**C1** is energetically preferred to *β*-**C1** for both studied series, Table S7 and Figure S19, Supporting Information.

Substituent effects on the monopalladation are easily seen in the corresponding computed $\Delta G^{\ddagger}$ values, which correlate nicely with the *para*-Hammett constants, showing the influence of the distant *para*-substituent, Table S8 and Figure S20, Supporting Information. Furthermore, the adducts *β*-**R** are about 3−10 kJ/mol less stable than *α*-**R**, Table S6, Supporting Information, whereas the $\Delta G^{\ddagger}$ values for the proton transfer from the phenyl rings to the coordinated DMF with respect to adducts are similar for the alpha and beta path (86.6−94.3 and 85.6−87.5 kJ/mol, respectively, Tables S6 and S8, Supporting Information). These data indicate that the stabilities of the reactants (adducts) and products (cyclopalladated complexes) dictate the overall regioselectivity of the monocyclopalladation reaction.

Dicyclopalladation. Optimized conformations of the species involved in the second palladation are analogous to those previously described for the monocyclopalladation process, Figure 6. *Cis*-transition states *α*-**C1**-**TS3** and *β*-**C1**-**TS3** are 15−22 kJ/mol more stable than the *trans*-transition states, Table S5 and Figure S16, Supporting Information. Smaller $\Delta_r G$ values for the cyclopalladated adduct formation than for the first adduct formation may be a reason for the slower second palladation reaction. In addition, the calculated results show significant differences between the alpha and beta paths in contrast to the monocyclopalladation. Alpha-adducts *α*-**C1**-**R** are 12−17 kJ/mol lower in energy than *β*-**C1**-**R**, while the energy barriers for the proton transfer from *α*-**C1**-**R** and *β*-

dx.doi.org/10.1021/ic402017v | Inorg. Chem. 2013, 52, 12749−12757

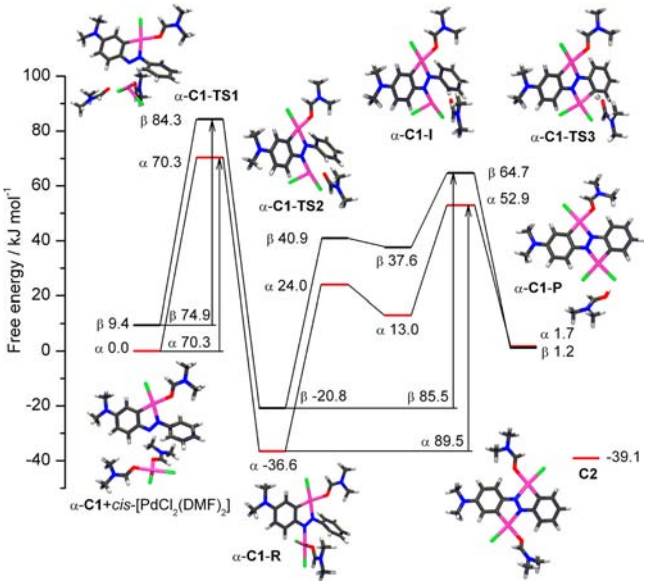

Figure 6. Energy profile for the dicyclopalladation reaction of **L7**. Alpha and beta paths are shown in red and black, respectively. Only alpha structures are drawn.

C1-R (89.5 and 85.5 kJ/mol, respectively) are close, Tables S6 and S8, Supporting Information. These findings along with the 9−14 kJ/mol differences in the energy barriers for the adduct formation in favor of the alpha path, Table S5, Supporting Information, lead to the faster conversion of *α*-**C1** to the dicyclopalladated complex **C2**.

Diadduct Cyclopalladation. The formation of diadducts $LPd_2Cl_4(DMF)_2$, with both azo-nitrogen atoms bonded to palladium atoms, Figure 7, is a possible concurrent reaction path that may occur after the formation of the *α*-**R** and *β*-**R** species, Scheme 2. Computed data show that $\Delta G^{\ddagger}$ values for the diadduct formation (83−89 kJ/mol, Table S5, Supporting Information) are close to $\Delta G^{\ddagger}$ for the cyclopalladation of *α*-**C1-R** (88−90 kJ/mol, Table S8, Supporting Information). Furthermore, palladation of the dimethylaminophenyl ring of

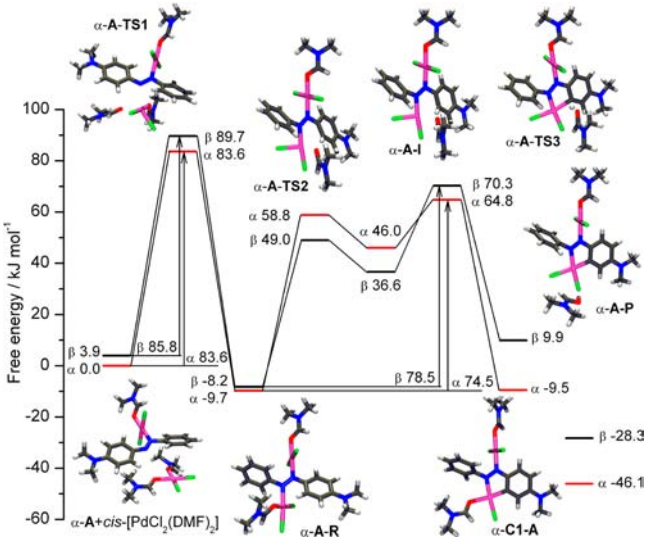

Figure 7. Energy profile for the diadduct cyclopalladation reaction of **L7**. Alpha and beta paths are shown in red and black, respectively. Only alpha structures are drawn.

α-**A-R** requires 73.2−76.2 kJ/mol, Table S8, Supporting Information, which is close to the activation barrier for the formation of the monocyclopalladated adduct (70.3−75.3 kJ/mol, Table S5, Supporting Information). We note here that the palladation of diadduct complexes proceeds from the species with at least one DMF molecule in the *cis* position toward the azobenzene, Figure S25 and Schemes S4 and S5, Supporting Information. The presented data show that the diadduct route to the dicyclopalladated complexes is energetically similar to the cyclopalladation of *α*-**C1**. Thus, diadduct reactions cannot be ruled out as the concurrent path from calculations alone, especially if we consider reaction conditions with a large molar excess of $PdCl_2(DMF)_2$. However, the results of the kinetic study discussed in the previous part exclude the second-order reaction with respect to palladium, indicating that this double adduct path is not preferred.

Finally, it should be noted that the computational results also could not explain the high reaction rates for the methyl orange (**L11**). The calculated $\Delta G^{\ddagger}$ for all studied reaction steps are strongly overestimated if compared with the data for other ligands and the experimental reaction rates, Table S8 and Figure S24, Supporting Information. PCM method allowed the modeling of the bulk solvent but without describing the specific interactions between the DMF molecules and the azobenzene or palladium species, which could influence the overall results. This also indicates that other effects, like solvent−solute interactions or dissociation of the ligand and subsequent changes in the ionic strength, may influence the reaction rates.

CONCLUSION

The well-known ability of azobenzene ligands to undergo cyclopalladation has been exploited to produce dicyclopalladated complexes that contain the planar Pd−azobenzene skeleton involving four fused rings, two phenyl rings and two palladacycles. The presence of these rings in dicyclopalladated complexes coupled with an electron-donating substituent on the phenyl rings in the *para* position significantly enhance their optical properties in comparison with the free ligands and monopalladated analogues.

The kinetics results, additionally supported by the Hammett correlations, have clearly demonstrated a strong effect of different 4,4′-substituents on the formation rate of mono- and dicyclopalladated azobenzenes. Experimental findings rationalized by the quantum-chemical calculations have strongly suggested that both cyclopalladations of azobenzenes consist of two successive steps: the first is the formation of adducts followed by the formation of the final (mono- or di-) cyclopalladated product. The reactivity of azobenzenes in mono- and dicyclopalladation is consistent with the mechanism that proceeds via electrophilic attack of palladium on the *ortho*-carbon of phenyl ring. The electrophilic C−H bond-activation pathways have been additionally supported by the quantum-chemical calculations and by the negative values of the Hammett correlation coefficients. This proton abstraction by the basic DMF ligand, which proceeds simultaneously with the formation of Pd−C bond, is the rate-determining step in both cyclopalladations.

The described results provide a better insight into the mechanism of mono- and dicyclopalladation of azobenzenes, the reactivity of all species involved in these reactions, and the role of the steric and electronic factors in the formation of palladacycles.

dx.doi.org/10.1021/ic402017v | *Inorg. Chem.* 2013, 52, 12749−12757

■ ASSOCIATED CONTENT

Supporting Information

Additional structural data for complexes **2**, **3′**, **5**, **6′**, and **8′**, along with the kinetics data, computational details including DFT geometries, and their energies. This material is available free of charge via the Internet at http://pubs.acs.org.

■ AUTHOR INFORMATION

Corresponding Authors

*E-mail: curic@irb.hr.

*E-mail: marina.juribasic@irb.hr.

Notes

The authors declare no competing financial interest.

■ ACKNOWLEDGMENTS

The Ministry of Science, Education and Sports of The Republic of Croatia (Grant Nos. 098-0982915-2950, 098-0982915-2945, and 006-0061247-0009) has provided financial support for this research. Computations were done on the Isabella cluster at SRCE, Zagreb. The authors would like to thank Tibor Kulcsár for help with the data processing and Prof. Mladen Biruš, Dr. Ivan Ljubić, and Prof. Vladislav Tomišić for valuable discussions.

■ REFERENCES

(1) Cope, A. C.; Siekman, R. W. *J. Am. Chem. Soc.* **1965**, *87*, 3272−3273.

(2) (a) Omae, I. *Coord. Chem. Rev.* **2004**, *248*, 995−1023. (b) Ryabov, A. D. *Synthesis* **1985**, 233−252. (c) Lyndon, D. P.; Rourke, J. P. *Chem. Commun.* **1997**, 1741−1742. (d) Hudson, S. A.; Maitlis, P. M. *Chem. Rev.* **1993**, *93*, 861−885. (e) Ghedini, M.; Aiello, I.; Crispini, A.; Golemme, A.; La Deda, M.; Pucci, D. *Coord. Chem. Rev.* **2006**, 1373−1390. (f) Bergbreiter, D. E.; Osburn, P. L.; Liu, Y. S. *J. Am. Chem. Soc.* **1999**, *121*, 9531−9538. (g) van der Boom, M. E.; Milstein, D. *Chem. Rev.* **2003**, *103*, 1759−1792. (h) Chen, C. L.; Liu, Y. H.; Peng, S. M.; Liu, S. T. *Organometallics* **2005**, *24*, 1075−1081. (i) Dupont, J.; Consorti, C. S.; Spencer, J. *Chem. Rev.* **2005**, *105*, 2527−2572. (j) Caires, A. C. F. *Anti-Cancer Agents. Med. Chem.* **2007**, *7*, 484−491. (k) Tušek-Božić, Lj.; Komac, M.; Ćurić, M.; Lyčka, A.; Scarcia, V.; Furlani, A. *Polyhedron* **2000**, *19*, 937−948.

(3) (a) Babić, D.; Ćurić, M.; Molčanov, K.; Ilc, G.; Plavec, J. *Inorg. Chem.* **2008**, *47*, 10446−10454. (b) Ćurić, M.; Babić, D.; Višnjevac, A.; Molčanov, K. *Inorg. Chem.* **2005**, *44*, 5975−5977.

(4) (a) Li, S.-H.; Yu, C.-W.; Xu, J.-G. *Chem. Commun.* **2005**, 450−452. (b) Juribašić, M.; Ćurić, M.; Molčanov, K.; Matković-Čalogović, D.; Babić, D. *Dalton Trans.* **2010**, *39*, 8769−8778 and references therein.

(5) (a) Cinčić, D.; Juribašić, M.; Babić, D.; Molčanov, K.; Šket, P.; Plavec, J.; Ćurić, M. *Chem. Commun.* **2011**, *47*, 11543−11545. (b) Wakatsuki, Y.; Yamazaki, H.; Grutsch, P. A.; Santhanam, M.; Kutal, C. *J. Am. Chem. Soc.* **1985**, *107*, 8153−8159.

(6) (a) Ćurić, M.; Babić, D.; Marinić, Ž.; Paša-Tolić, Lj.; Butković, V.; Plavec, J.; Tušek-Božić, Lj. *J. Organomet. Chem.* **2003**, *687*, 85−99. (b) Sinha, C.; Bandyopadhyay, D.; Chakravorty, A. *Inorg. Chem.* **1988**, *27*, 1173−1178. (c) Omae, I. *Chem. Rev.* **1979**, *79*, 287−321. (f) Bruce, M. I. *Angew. Chem., Int. Ed.* **1977**, *16*, 73−86. (d) Dehand, J.; Pfeffer, M. *Coord. Chem. Rev.* **1976**, *18*, 327−352.

(7) (a) Albrecht, M. *Chem. Rev.* **2010**, *110*, 576−623. (b) Ryabov, A. D.; Sakodinskaya, I. K.; Yatsimirski, A. K. *J. Chem. Soc., Dalton Trans.* **1985**, 2629−2638. (c) Yagyu, T.; Aizawa, S.; Funahashi, S. *Bull. Chem. Soc. Jpn.* **1998**, *71*, 619−629. (d) Yagyu, T.; Iwatsuki, S.; Aizawa, S.; Funahashi, S. *Bull. Chem. Soc. Jpn.* **1998**, *71*, 1857−1862. (e) Gomez, M.; Granell, J.; Martinez, M. *Eur. J. Inorg. Chem.* **2000**, 217−224.

(8) Babić, D.; Ćurić, M.; Smith, D. M. *J. Organomet. Chem.* **2011**, *696*, 661−669.

(9) (a) Parshall, G. W. *Acc. Chem. Res.* **1970**, *3*, 139−144. (b) Bruce, M. I.; Goodall, B. L.; Stone, G. A. *J. Chem. Soc., Dalton Trans.* **1978**, 687−694.

(10) (a) *CrysAlisPRO*, Oxford Diffraction Ltd., Oxford, U.K., 2007. (b) Sheldrick, G. M. *SHELX97, Programs for Crystal Structure Analysis*, release 97-2, Universität Göttingen, Germany, 1997. (c) Sheldrick, G. M. *SHELXL97, Program for Refinement of Crystal Structures*, Universität Göttingen, Germany, 1997. (d) Spek, A. L. *PLATON98: A Multipurpose Crystallographic Tool*, 120398 version, University of Utrecht, Netherlands, 1998. (e) Farrugia, L. J. *J. Appl. Crystallogr.* **1997**, *30*, 565−566. (f) McCabe, P.; Pidcock, E.; Shields, G. P.; Taylor, R.; Towler, M.; Macrae, C. F.; Edgington, P. R.; Van de Streek, J. *J. Appl. Crystallogr.* **2006**, *39*, 453−457.

(11) Frisch, M. J.; Trucks, G. W.; Schlegel, H. B.; Scuseria, G. E.; Robb, M. A.; Cheeseman, J. R.; Scalmani, G.; Barone, V.; Mennucci, B.; Petersson, G. A.; Nakatsuji, H.; Caricato, M.; Li, X.; Hratchian, H. P.; Izmaylov, A. F.; Bloino, J.; Zheng, G.; Sonnenberg, J. L.; Hada, M.; Ehara, M.; Toyota, K.; Fukuda, R.; Hasegawa, J.; Ishida, M.; Nakajima, T.; Honda, Y.; Kitao, O.; Nakai, H.; Vreven, T.; Montgomery, J. A., Jr.; Peralta, J. E.; Ogliaro, F.; Bearpark, M.; Heyd, J. J.; Brothers, E.; Kudin, K. N.; Staroverov, V. N.; Kobayashi, R.; Normand, J.; Raghavachari, K.; Rendell, A.; Burant, J. C.; Iyengar, S. S.; Tomasi, J.; Cossi, M.; Rega, N.; Millam, J. M.; Klene, M.; Knox, J. E.; Cross, J. B.; Bakken, V.; Adamo, C.; Jaramillo, J.; Gomperts, R.; Stratmann, R. E.; Yazyev, O.; Austin, A. J.; Cammi, R.; Pomelli, C.; Ochterski, J. W.; Martin, R. L.; Morokuma, K.; Zakrzewski, V. G.; Voth, G. A.; Salvador, P.; Dannenberg, J. J.; Dapprich, S.; Daniels, A. D.; Farkas, O.; Foresman, J. B.; Ortiz, J. V.; Cioslowski, J.; Fox, D. J. *Gaussian 09*, revision A.02; Gaussian, Inc.: Wallingford, CT, 2009.

(12) (a) Stephens, P. J.; Devlin, F. J.; Chabalowski, C. F.; Frisch, M. J. *J. Phys. Chem.* **1994**, *98*, 11623−11627. (b) Andrae, D.; Haussermann, U.; Dolg, M.; Stoll, H.; Preuss, H. *Theor. Chim. Acta* **1990**, *77*, 123−141. (c) Miertus, S.; Scrocco, E.; Tomasi, J. *Chem. Phys.* **1981**, *55*, 117−129. (d) Fukui, K. *Acc. Chem. Res.* **1981**, *14*, 363−368.

(13) Molčanov, K.; Ćurić, M.; Babić, D.; Kojić-Prodić, B. *J. Organomet. Chem.* **2007**, *692*, 3874−3881.

(14) Hansch, C.; Leo, A.; Taft, R. W. *Chem. Rev.* **1991**, *91*, 165−195.